Intermetallics 136 (2021) 107234

Contents lists available at ScienceDirect

Intermetallics

journal homepage: www.elsevier.com/locate/intermet

Pronounced β-relaxation in plastic FeNi-based bulk metallic glasses and its structural origin

Jing Zhou [a,b,c], Si-Yi Di [d], Bao-An Sun [c,e], Rui Zhao [e], Qiao-Shi Zeng [d], Jian-Guo Wang [a], Zhen-Zhong Sun [a], Wei-Hua Wang [c,e], Bao-Long Shen [d,f,*]

[a] School of Mechanical Engineering, Dongguan University of Technology, Dongguan 523808, China
[b] State Key Laboratory for Mechanical Behaviour of Materials, Xi'an Jiaotong University, Xi'an 710049, China
[c] Songshan Lake Materials Laboratory, Dongguan, Guangdong 523808, China
[d] School of Materials Science and Engineering, Jiangsu Key Laboratory for Advanced Metallic Materials, Southeast University, Nanjing 211189, China
[e] Institutes of Physics, Chinese Academy of Sciences, Beijing 100190, China
[f] Institute of Massive Amorphous Metal Science, China University of Mining and Technology, Xuzhou, 221116, China

ARTICLE INFO

Keywords:
FeNi-Based BMG
β-relaxation
Plasticity
Structural heterogeneity
Atomic-scale structure

ABSTRACT

Fe-based bulk metallic glasses (BMGs) usually exhibit brittle behavior and unconspicuous β-relaxation in their dynamic mechanical spectroscopy. We report a distinct β-relaxation behavior in FeNi-based BMGs with excellent plasticity. The origin of pronounced β-relaxation and plastic behaviors for the FeNi-based BMGs were investigated by synchrotron X-ray diffraction and nanoindentation tests in detail. It is found that the structural heterogeneity plays a key role in the dynamic of the FeNi-based BMGs, leading to large amount of loosely packed regions. The pronounced β-relaxation is also found to have a good correlation with the plasticity for the FeNi-based BMGs. This study might provide guidance for us to develop plastic BMGs from an atomic structural and glass dynamic perspective.

1. Introduction

Since the FePC metallic glass (MG) first developed in 1967 [1], a large number of Fe-based MGs with excellent magnetic properties such as high saturation magnetic flux density, low coercivity and low core loss have been developed [2–4]. Among them, the representative FeNi-based MGs with better high frequency characteristics have been used to substitute permalloys in sensors, switching transformer, anti-theft label etc, under the trademark of METGLAS2826 [5]. The attractive properties of FeNi-based BMGs including high strength, high elastic limit, excellent soft magnetic properties, high-efficient degrading ability and excellent corrosion resistance significantly expand their potential application fields [6–10]. However, due to the poor plasticity at room temperature, the application of the BMGs as structural and functional materials is restricted.

The plastic deformation in BMGs is accomplished by the cooperative shearing of atomic clusters termed as shear transformation zones (STZs) [11]. Such zones can accommodate the shear strain under loading, and often starts from the loosely packed regions in BMGs [12,13]. In addition, recent studies have indicated that the activation energy of STZs is almost equal to activation of β-relaxation [14–16]. It means that this local collective motion of atoms provides the source of β-relaxation, as well as the sites for potential STZs. Very recently, Wang et al. claimed that the β-relaxation in FeZrB MG is related to the heterogeneous structure with plenty of loosely packed zones [17], which is effective to improve the plasticity of Fe-based MGs. Thus, Fe-based BMGs with distinct β-relaxation are expected to have large number of potential STZ sites to accommodate plastic deformation and they may exhibit good plasticity. However, the β-relaxation behaviors of most Fe-based BMGs are rather ambiguous, and most of them are merged into the α-relaxation [18]. This restricts the development of plastic Fe-based BMGs from the perspective of relaxation dynamics as experienced in other BMG systems, and limits the experimental study and the understanding of the nature of β-relaxation in Fe-based BMG.

In this work, the FeNiBSiPNb BMG with excellent soft magnetic properties was selected as the base alloy to develop plastic FeNi-based BMG from perspective of β-relaxation [19]. By adjusting the P/B atomic ratio in this base alloy, a $Fe_{39}Ni_{39}B_{16.95-x}Si_{2.75}Nb_{2.3}P_x$ (x = 1.38, 2.75, 4.13, 5.5, 6.88 and 8.25 at.%) BMG system with pronounced β-relaxation behaviors and excellent mechanical peoperties were

* Corresponding author. Institute of Massive Amorphous Metal Science, China University of Mining and Technology, Xuzhou, 221116, China.
E-mail address: blshen@seu.edu.cn (B.-L. Shen).

https://doi.org/10.1016/j.intermet.2021.107234
Received 23 March 2021; Received in revised form 26 April 2021; Accepted 2 May 2021
Available online 2 June 2021

successfully developed. The detailed investigations were carried out to study the effects of P addition on β-relaxation behavior and mechanical peoperties of FeNiBSiPNb BMGs from an atomic-structure perspective. The results suggest that the structural heterogeneity plays a critical role in plastic and dynamic behaviors in Fe-based BMGs, and the increasing heterogeneity causes the more pronounced β-relaxation, thereby leading to the large plasticity. It provides an avenue to design the plasticity of Fe-based BMGs from the perspective of relaxation dynamics.

2. Materials and methods

2.1. Sample preparation

Alloy ingots of $Fe_{39}Ni_{39}B_{16.95-x}Si_{2.75}Nb_{2.3}P_x$ (x = 1.38, 2.75, 4.13, 5.5, 6.88 and 8.25 at.%) were prepared by induction melting of high-purity Fe (99.99%), Ni (99.99%), B (99.99%), Si (99.999%), Nb (99.95%) and pre-alloyed Fe–P ingots that consist of 75% Fe and 25% P in a purified argon atmosphere. Ribbon samples were produced by single roller melt-spinning method with thickness of 25 μm and width of 1.2 mm. Cylindrical rods with diameters of 1–2.5 mm were produced by copper mold casting in a pure argon atmosphere. The amorphous structure of ribbon and rod samples was confirmed by X-ray diffraction (XRD) employing a Bruker AXS (D8-Discover) instrument with CuKα radiation.

2.2. Sample characterization

Thermal properties including glass transition temperature (T_g), crystallization temperature (T_x), supercooled liquid region ($\triangle T_x = T_x - T_g$), and exothermic heat of relaxation ($\triangle H_{rel}$) were measured using differential scanning calorimetry (DSC, NETZSCH DSC404F3) at a heating rate of 0.67 K/s. The liquidus temperature (T_l) was measured using a DSC by cooling the molten samples at a cooling rate of 0.067 K/s. The dynamical mechanical spectrums of the FeNi-based BMGs were carried out under a dynamical mechanical analyzer (DMA, NETZSCH 242 E) by single cantilever bending mode at a frequency of 1 Hz and a constant heating rate of 3 K/min. Specimens with dimension of 30 × 1 × 1 mm^3 were prepared for the DMA measurements.

The structure of all samples was then tested by synchrotron radiation XRD with a wavelength of 0.117418 Å by using beam line 11-IDC in the Advanced Photon Source of USA. A Mar345 image plate was used to record two dimensional diffraction data. Subsequently, the diffraction data were normalized by software PDFgetX2 to get structure factors $S(Q)$ and corresponding pair distribution functions $G(r)$ [20,21]. Indentation tests were conducted using NanoTest Vantage (Micro Materials Ltd) with a Berkovich diamond tip. The indentations were performed in load control mode. Starting with a linear ramp up to the maximum load of 50 mN at the a loading rate of 1 mN/s, the loading course was continued by holding the maximum load for 100 s, and finally by unloading to zero load at a loading rate of 1 mN/s. The middle area of each sample was mapped by 64 indentations with 30 μm spacing in the radial direction and 30 μm over the height. Hardness values were determined using the standard Oliver-Pharr method [22]. The 100 s hold segment at maximum load was to minimize the influence of creep during unloading; a 30 s hold segment at 10% of maximum load was for thermal drift correction. The plastic strain (ϵ_p) and yield strength (σ_y) were measured through compressive testing by using a Sans 5305 testing machine at room temperature with a strain rate of 5×10^{-4} s^{-1}. The samples with 1 mm in diameter and 2 mm in length were cut from the as-cast glassy rods. A custom designed device was used to polish the ends of the samples to ensure that the ends are parallel and perpendicular to the lateral surfaces.

3. Results and discussion

The amorphous structure of all the ribbon samples used for thermal tests are comfirmed by XRD measurement. Fig. 1a shows the DSC curves of $Fe_{39}Ni_{39}B_{16.95-x}Si_{2.75}Nb_{2.3}P_x$ (x = 1.38, 2.75, 4.13, 5.5, 6.88 and 8.25 at.%) MGs. As shown in the figure, the curves for all the ribbons present a large supercooled liquid region. Table 1 summarizes the thermal parameters of the $Fe_{39}Ni_{39}B_{16.95-x}Si_{2.75}Nb_{2.3}P_x$ MGs. It can be seen that the T_g decreases from 722 to 703 K with the increasing of P content from x = 1.38 to 8.25. However, the T_x increases gradually from 753 to 761 K, with P content from x = 1.38 to 4.13, and then decreases slightly to 754 K with further increasing P content to x = 8.25. As a result, the ΔT_x increases from 31 to 51 K with increasing the P content, indicating the improvement of thermal stability of FeNi-based MG during the supercooled liquid region. Fig. 1b shows DCS curves of cooling behavior for

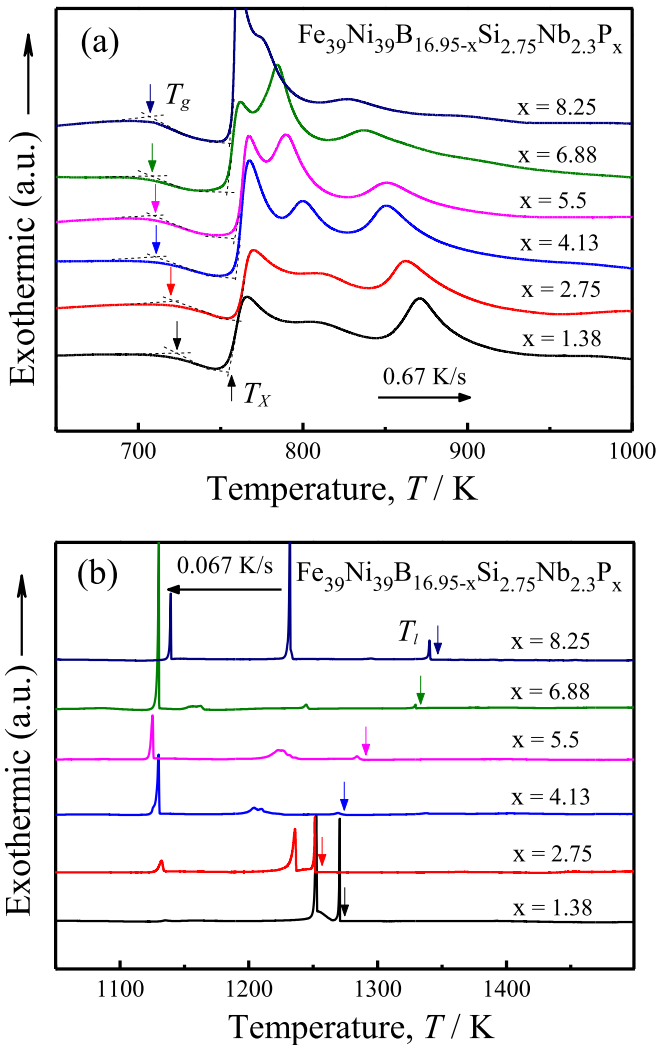

Fig. 1. DSC curves of $Fe_{39}Ni_{39}B_{16.95-x}Si_{2.75}Nb_{2.3}P_x$ (x = 1.38, 2.75, 4.13, 5.5, 6.88 and 8.25 at.%) MG ribbons: (a) during heating process; (b) during cooling process.

Table 1
Thermal parameters of $Fe_{39}Ni_{39}B_{16.95-x}Si_{2.75}Nb_{2.3}P_x$ (x = 1.38, 2.75, 4.13, 5.5, 6.88 and 8.25 at.%) MG ribbons.

P Content(at.%)	T_g(K)	T_x(K)	T_l(K)	$\triangle T_x$(K)
1.38	722	753	1272	31
2.75	720	760	1253	40
4.13	75	761	1276	46
5.5	710	759	1290	49
6.88	706	755	1335	49
8.25	703	754	1341	51

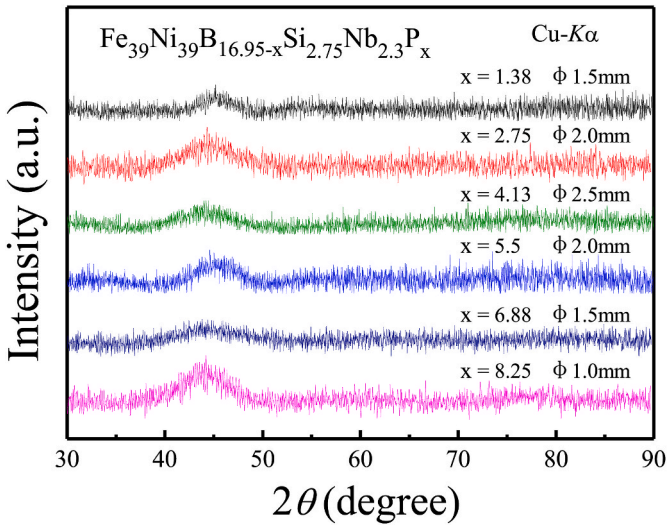

Fig. 2. XRD patterns of as-cast $Fe_{39}Ni_{39}B_{16.95-x}Si_{2.75}Nb_{2.3}P_x$ (x = 1.38, 2.75, 4.13, 5.5, 6.88 and 8.25 at.%) BMGs with corresponding critical maximum diameters.

these $Fe_{39}Ni_{39}B_{16.95-x}Si_{2.75}Nb_{2.3}P_x$ MGs. It can be seen that T_l decreases from 1272 to 1253 K with the increasing of P content from x = 1.38 to 2.75, and then slightly increases to 1341 K when x = 8.25. In addition, the temperature interval between the three exothermic reaches the minimum value at x = 2.75, indicated that the $Fe_{39}Ni_{39}B_{14.2}Si_{2.75}Nb_{2.3}P_{2.75}$ MG approaches a eutectic point [23].

Based on the DSC results, we expect that this $Fe_{39}Ni_{39}B_{16.95-x}Si_{2.75}Nb_{2.3}P_x$ system will exhibit a large glass forming ability (GFA). Thus, we tried to use copper mold casting method to cast BMG samples of different diameters. As a result, all compositions for $Fe_{39}Ni_{39}B_{16.95-x}Si_{2.75}Nb_{2.3}P_x$ MG system can form BMG rods with diameters from 1 to 2.5 mm. Fig. 2 shows the XRD patterns of $Fe_{39}Ni_{39}B_{16.95-x}Si_{2.75}Nb_{2.3}P_x$ BMG with critical diameters. It is clear that all the curves only contained broad peaks without crystalline peaks, indicating the formation of fully amorphous structure. Thus, we can claim that the critical diameter for $Fe_{39}Ni_{39}B_{16.95-x}Si_{2.75}Nb_{2.3}P_x$ system was 1 mm at x = 8.25, 1.5 mm at x = 1.38 and 6.88, 2 mm at x = 5.5, 2.5 mm at x = 2.75 and 4.13, respectively.

Here we analyze the effects of P content on GFA in the $Fe_{39}Ni_{39}B_{16.95-x}Si_{2.75}Nb_{2.3}P_x$ MG system. Firstly, the constituent elements of this MG system have big atomic size mismatch with a combination of large atoms (Fe, Ni, Nb) and small atoms (P, B, Si). Secondly, the mixing enthalpies for P–Ni (−26), P–Fe (−31), P–Nb (−81) and P–Si (−25.5) atomic pairs are almost three times larger than those for B–Ni (−9), B–Fe (−11), B–Nb (−39) and B–Si (−14) atomic pairs [24]. It has been pointed out that the large (L) and small (S) atoms with large negative mixing enthalpies may form a strong L-S reinforced "backbone" structure, leading to a highly stable undercooled liquid, and further suppresses crystallization [25]. Thus, proper P/B atomic ratio can effectively enhance the GFA of FeNiBSiPNb glassy system. In addition, another reason considered here is that the proper P/B atomic ratio brings the alloy composition close to the eutectic point, leading to the enhancement of GFA. In a word, the $Fe_{39}Ni_{39}B_{16.95-x}Si_{2.75}Nb_{2.3}P_x$ glassy system shows strong GFA and can be casted into bulk amorphous alloy samples.

In addition, we also measured their relaxation behaviors by DMA using the rod sample with 1 mm in diameter. Fig. 3a shows the temperature dependences of the loss modulus E'' for $Fe_{39}Ni_{39}B_{16.95-x}Si_{2.75}Nb_{2.3}P_x$ (x = 1.38, 4.13 and 6.88 at.%) BMGs in a normalized frame where T and E'' are scaled by the T_g and the maximum loss modulus, respectively. As shown in the elliptical region of Fig. 3a, the intensity of β-relaxation increases with the increase of P comtent, indicating that the $Fe_{39}Ni_{39}B_{10.07}Si_{2.75}Nb_{2.3}P_{6.88}$ BMG shows the most

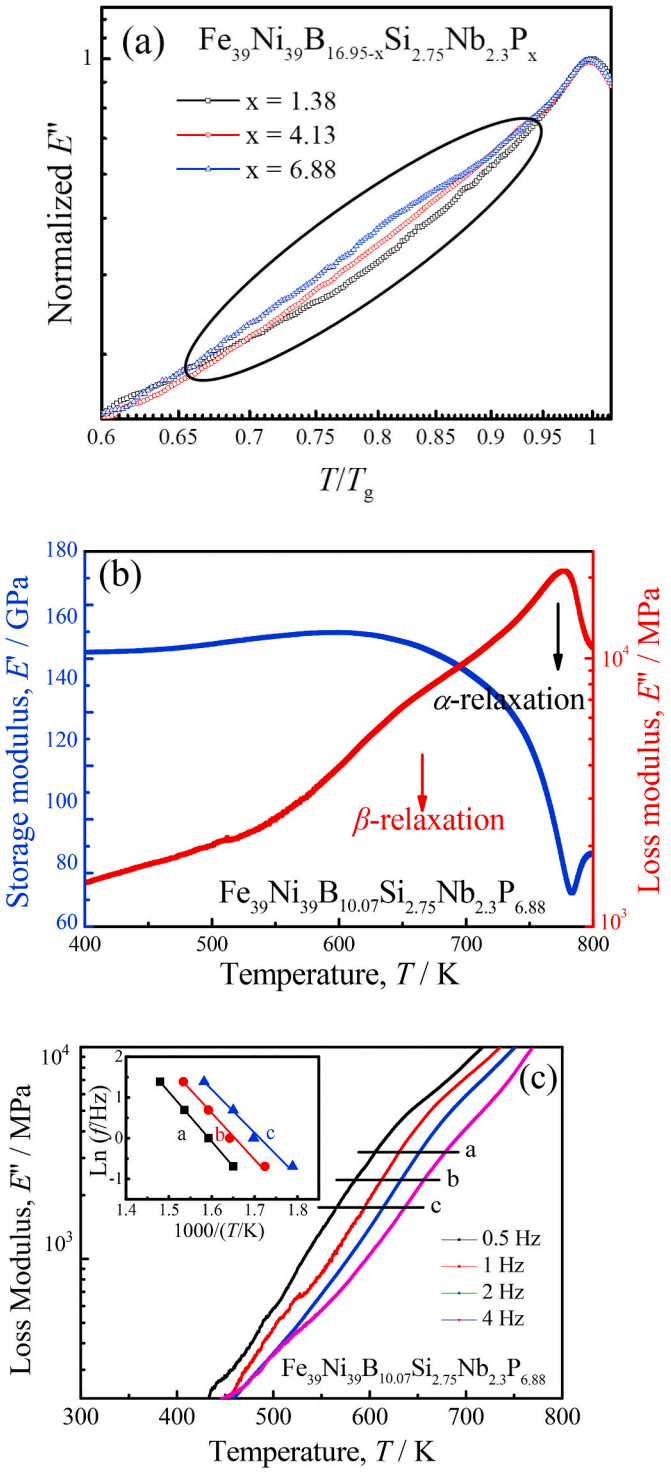

Fig. 3. (a) Normalized loss modulus curves at 1 Hz for $Fe_{39}Ni_{39}B_{16.95-x}Si_{2.75}Nb_{2.3}P_x$ (x = 1.38, 4.13 and 6.88 at.%) BMGs; (b) Temperature dependence of the loss modulus E'' and storage modulus E' for $Fe_{39}Ni_{39}B_{10.07}Si_{2.75}Nb_{2.3}P_{6.88}$ BMG at a frequency of 1 Hz and heating rate of 3 K/min. (c) Temperature dependence of the peak frequency of β-relaxation in $Fe_{39}Ni_{39}B_{10.07}Si_{2.75}Nb_{2.3}P_{6.88}$ BMG. The inset is the temperature dependence of the peak frequence of β-relaxation in $Fe_{39}Ni_{39}B_{10.07}Si_{2.75}Nb_{2.3}P_{6.88}$ BMG.

pronounced β-relaxation among the studied BMG system. To further confirm β-relaxation behavior, the temperature dependence of the loss modulus E'' and storage modulus E' for $Fe_{39}Ni_{39}B_{10.07}Si_{2.75}Nb_{2.3}P_{6.88}$ BMG is shown in Fig. 3b. Obviously, a distinct slow β-relaxation peak is observed at about 650 ± 3 K. Both of the α-relaxation and β-relaxation

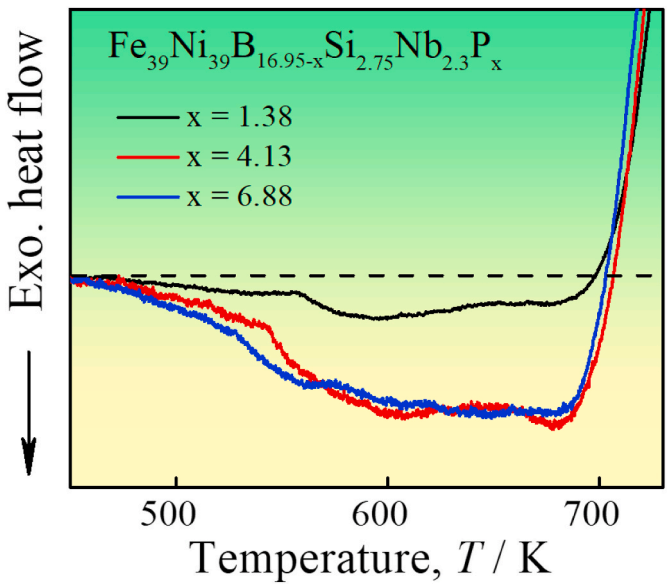

Fig. 4. The relaxation spectra for the $Fe_{39}Ni_{39}B_{16.95-x}Si_{2.75}Nb_{2.3}P_x$ (x = 1.38, 4.13 and 6.88 at.%) BMGs.

peaks have a corresponding drop in E' curve. Fig. 3c shows the temperature dependences of the loss modulus $E''$for $Fe_{39}Ni_{39}B_{10.07}Si_{2.75}Nb_{2.3}P_{6.88}$ BMG at various frequency (f) ranging from 0.5 to 4 Hz. It can be seen that the β-relaxation shifts to a higher temperature with the increase of f. Its activation energy, E_β, can be estimated by plotting ln(f) versus 1000/T_β. The inset of Fig. 3c exhibits the Arrhenius fit of $Fe_{39}Ni_{39}B_{10.07}Si_{2.75}Nb_{2.3}P_{6.88}$ BMG with three measured sets of data. Since the peak temperatures of β-relaxation in the present case were difficult to determine, we drew a horizontal line within the range where the β-relaxation occurred, each intersection with individual E'' curve defined values of frequency and temperature, and ultimately these values were used to determine the E_β instead of the peak data [17]. Using this method, Its E_β is determined to be 124 kJ/mol, or $E_\beta = 21.3\ (\pm 1.6)\ RT_g$ (R is the gas constant), which is roughly in agreement with the relationship found between the E_β and T_g in various MGs [17,18]. It is worthy mentioned that such a FeNi-based BMG without rare earth element, combined with large GFA and pronounced β-relaxation has never been reported before.

The results of DMA demonstrate the behaviors of β-relaxation in $Fe_{39}Ni_{39}B_{16.95-x}Si_{2.75}Nb_{2.3}P_x$ system are significantly affected by the composition of samples. A pertinent question is what is the origin of complicated chemical effect in the FeNi-based BMGs. It has been reported that different atomic-scale structures alter the energy state of MGs and affect the dynamic behaviour of BMGs differently [18,26,27]. Such differences in atomic-sacle structure can be evaluated by monitoring the changes of $\triangle H_{rel}$ on heating up to T_g [28]. Fig. 4 shows the exothermic signals before glass transition in DSC curves of $Fe_{39}Ni_{39}B_{16.95-x}Si_{2.75}Nb_{2.3}P_x$ BMGs. The exothermic heat of relaxation $\triangle H_{rel}$ determined by the enclosed areas increase from 0.053 to 0.151 kJ/mol with increasing the P content from 1.38 to 6.88 at.%, indicating that the enthalpies increase with the increase of P content, resulting in more loosely packed regions have been introduced in $Fe_{39}Ni_{39}B_{10.07}Si_{2.75}Nb_{2.3}P_{6.88}$ BMG.

It should be noted that the obtained evidence from DSC for the amount of loosely packed regions varied with the composition is indirect. Thus, the synchrotron XRD measurements were performed to see the changes of atomic-scale sturucture in FeNi-based BMGs more quantitatively. Fig. 5a shows the total structure factor ($S(Q)$) of glassy $Fe_{39}Ni_{39}B_{16.95-x}Si_{2.75}Nb_{2.3}P_x$ MG, which exhibits noticeable changes in the first peaks among three samples. For clarity, the inset in Fig. 5a shows the zoomed-in first peak, which increases in intensity by 10.2%

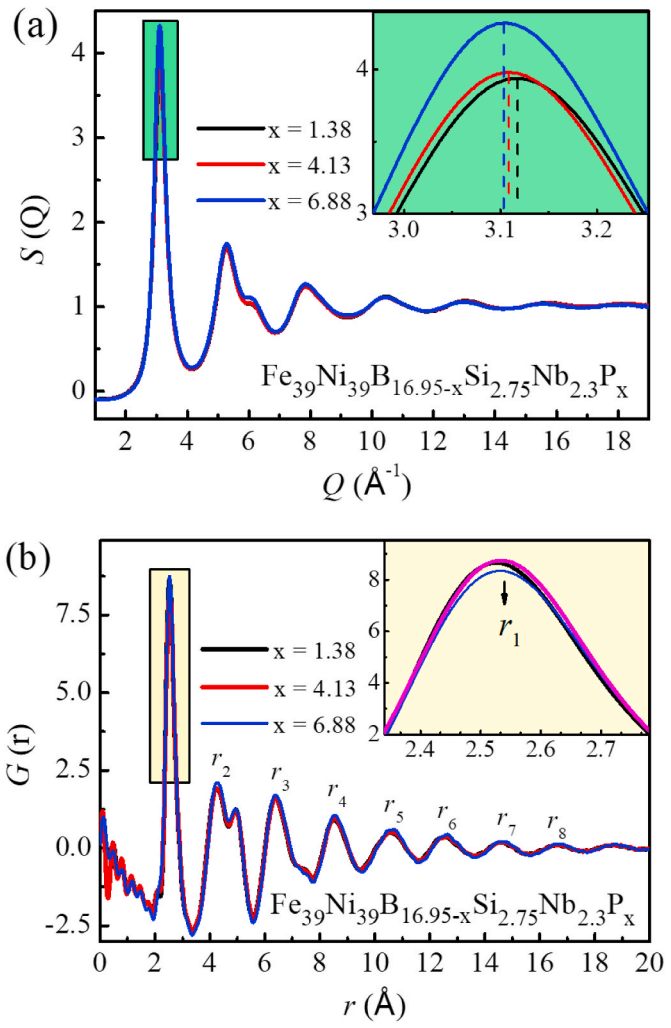

Fig. 5. Synchrotron XRD results of $Fe_{39}Ni_{39}B_{16.95-x}Si_{2.75}Nb_{2.3}P_x$ (x = 1.38, 4.13 and 6.88 at.%) MGs. (a) Total structure factor $S(Q)$, inset is the enlarge region on the first peak of $S(Q)$ shown in (a) with dashed lines denoting the peak positions. (b) Reduced pair distribution function $G(r)$, inset is the enlarge region on the first peak of $G(r)$ shown in (b) with dashed lines denoting the peak positions.

from $S(Q_{x=1.38}) = 3.93$ for $Fe_{39}Ni_{39}B_{15.57}Si_{2.75}Nb_{2.3}P_{1.38}$ MG to $S(Q_{x=6.88}) = 4.33$ for $Fe_{39}Ni_{39}B_{10.07}Si_{2.75}Nb_{2.3}P_{6.88}$ MG, and shifts slightly from $Q_{x=1.38} = 3.104$ Å^{-1} for $Fe_{39}Ni_{39}B_{15.57}Si_{2.75}Nb_{2.3}P_{1.38}$ MG to $Q_{x=6.88} = 3.118$ Å^{-1} for $Fe_{39}Ni_{39}B_{10.07}Si_{2.75}Nb_{2.3}P_{6.88}$ MG, respectively. The highest intensity of first peak indicates the highest pronounced topological ordering in $Fe_{39}Ni_{39}B_{10.07}Si_{2.75}Nb_{2.3}P_{6.88}$ MG. In addition, the decreasing value of Q position indicates an increasing tendency of mean atomic distance with the increasing P content [29], which means the larger amount of loosely packed regions stored in $Fe_{39}Ni_{39}B_{10.07}Si_{2.75}Nb_{2.3}P_{6.88}$ MG. The $G(r)$ curves of $Fe_{39}Ni_{39}B_{16.95-x}Si_{2.75}Nb_{2.3}P_x$ MGs were calculated by the Fourier transform from the corresponding $S(Q)$ curves, as shown as Fig. 5b. It can be seen that the intensity of r_1 to r_8 peaks increases with the increase P content, indicating higher degree of structural ordering in short to medium-range-scale of $Fe_{39}Ni_{39}B_{10.07}Si_{2.75}Nb_{2.3}P_{6.88}$ MG. Thus, it is clear that adjusting the P/B atomic ratio can effectively change the atomic-sacle structure of $Fe_{39}Ni_{39}B_{16.95-x}Si_{2.75}Nb_{2.3}P_x$ system, leading to the more pronounced atomic-scale structural heterogeneity existing in the $Fe_{39}Ni_{39}B_{10.07}Si_{2.75}Nb_{2.3}P_{6.88}$ MG.

Furthermore, the nanoindentation tests are carried out to investigate the structural heterogeneity at mesoscale. The values of hardness (H) for

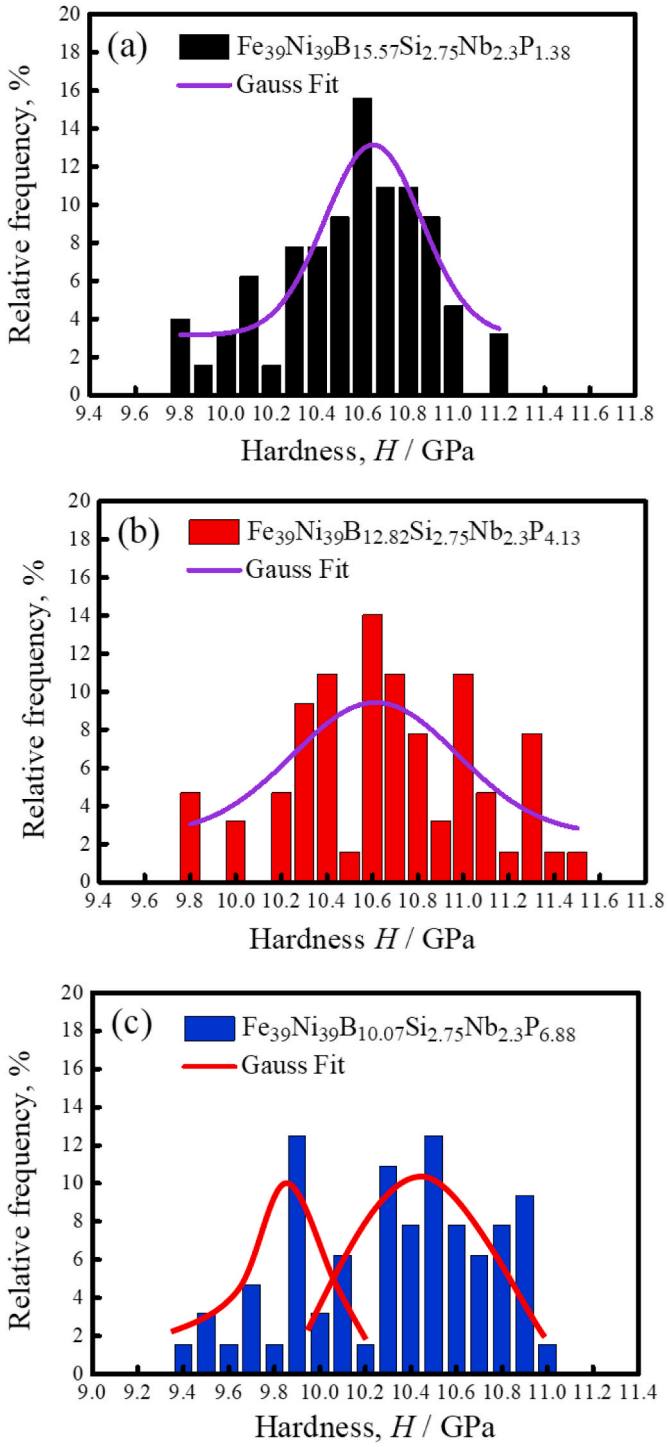

Fig. 6. The distributions of the reduced nanoindentation hardness: (a) for $Fe_{39}Ni_{39}B_{15.57}Si_{2.75}Nb_{2.3}P_{1.38}$ BMG; (b) for $Fe_{39}Ni_{39}B_{12.82}Si_{2.75}Nb_{2.3}P_{4.13}$ BMG; (c) for $Fe_{39}Ni_{39}B_{10.07}Si_{2.75}Nb_{2.3}P_{6.88}$ BMG.

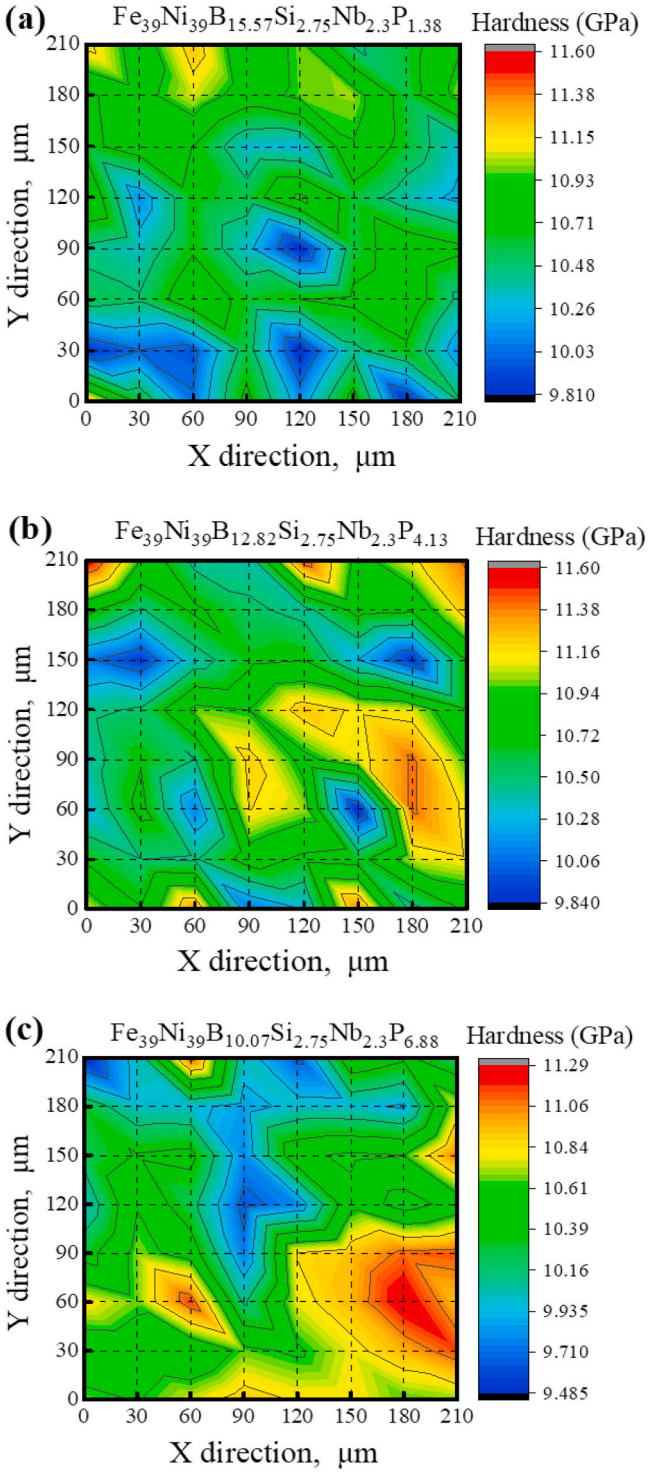

Fig. 7. The contour-line maps of the nanoindentation hardness values over a square area on the surface of the $Fe_{39}Ni_{39}B_{16.95-x}Si_{2.75}Nb_{2.3}P_x$ (x = 1.38, 4.13 and 6.88 at.%) BMGs shows the microscale mechanical heterogeneity: (a) for $Fe_{39}Ni_{39}B_{15.57}Si_{2.75}Nb_{2.3}P_{1.38}$ BMG; (b) for $Fe_{39}Ni_{39}B_{12.82}Si_{2.75}Nb_{2.3}P_{4.13}$ BMG; (c) for $Fe_{39}Ni_{39}B_{10.07}Si_{2.75}Nb_{2.3}P_{6.88}$ BMG.

$Fe_{39}Ni_{39}B_{16.95-x}Si_{2.75}Nb_{2.3}P_x$ BMGs are $10.72^{+0.48}_{-0.92}$, $10.67^{+0.83}_{-0.87}$ and $10.46^{+0.54}_{-1.06}$, respectively, which were obtained by fitting the nanoindentation curves. A decreasing average nanohardness with increasing P content are observed, which further confirms that a looser structure is frozen in FeNi-based BMGs with higher P content [30,31]. Fig. 6 characterizes the statistical distribution of nanohardness for these FeNi-based BMGs. It is clear seen that the nanohardness mainly distributes between 9.8 and 11.4 GPa for $Fe_{39}Ni_{39}B_{15.57}Si_{2.75}Nb_{2.3}P_{1.38}$ BMG, 9.8 and 11.5 GPa for $Fe_{39}Ni_{39}B_{12.82}Si_{2.75}Nb_{2.3}P_{4.13}$ BMG, 9.4 and 11 GPa for $Fe_{39}Ni_{39}B_{10.07}Si_{2.75}Nb_{2.3}P_{6.88}$ BMG, which means that the $Fe_{39}Ni_{39}B_{12.82}Si_{2.75}Nb_{2.3}P_{4.13}$ BMG and $Fe_{39}Ni_{39}B_{10.07}Si_{2.75}Nb_{2.3}P_{6.88}$ BMG have a wider distribution of nanohardness than $Fe_{39}Ni_{39}B_{15.57}Si_{2.75}Nb_{2.3}P_{1.38}$ BMG. In addition, the highest fraction peak value is 15.6 for $Fe_{39}Ni_{39}B_{15.57}Si_{2.75}Nb_{2.3}P_{1.38}$ BMG when H = 10.5 GPa, 14 for $Fe_{39}Ni_{39}B_{12.82}Si_{2.75}Nb_{2.3}P_{4.13}$ BMG when H = 10.6 GPa, and 12.5 for

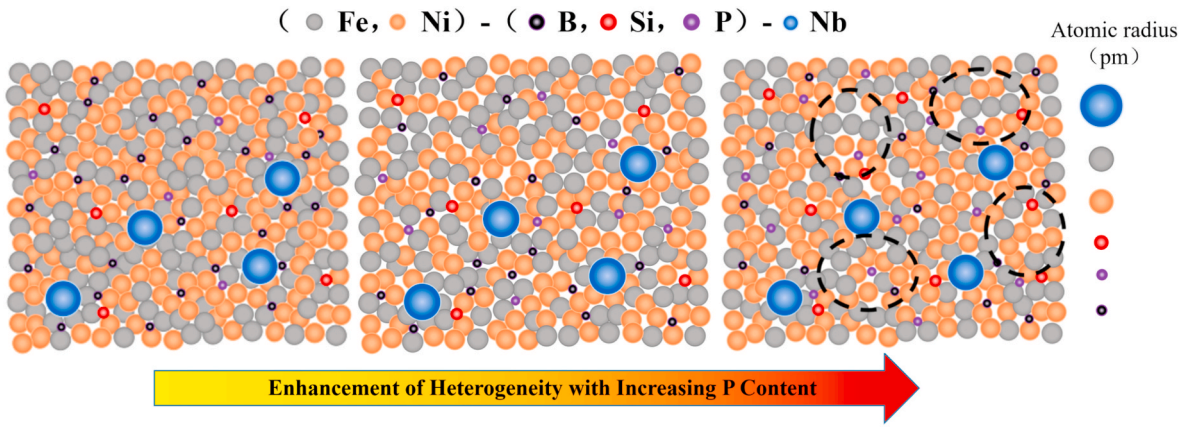

Fig. 8. Schematic diagram illustrating the atomic-scale structure of $Fe_{39}Ni_{39}B_{16.95-x}Si_{2.75}Nb_{2.3}P_x$ (x = 1.38, 4.13 and 6.88 at.%) BMGs.

$Fe_{39}Ni_{39}B_{10.07}Si_{2.75}Nb_{2.3}P_{6.88}$ BMG when H = 9.9 and 10.5 GPa, indicating that the $Fe_{39}Ni_{39}B_{10.07}Si_{2.75}Nb_{2.3}P_{6.88}$ BMG has a more dispersive hardness throughout the whole sample. The dispersed nanohardness data confirm the existence of hard and soft regions. Wang et al. pointed out that the regions with more loosely packed structure possessed "liquid-like" property such as low hardness and modulus [30,32]. From above results, the $Fe_{39}Ni_{39}B_{10.07}Si_{2.75}Nb_{2.3}P_{6.88}$ BMG exhibits higher degree of mechanical heterogeneity. It is worthy mentioned that there is

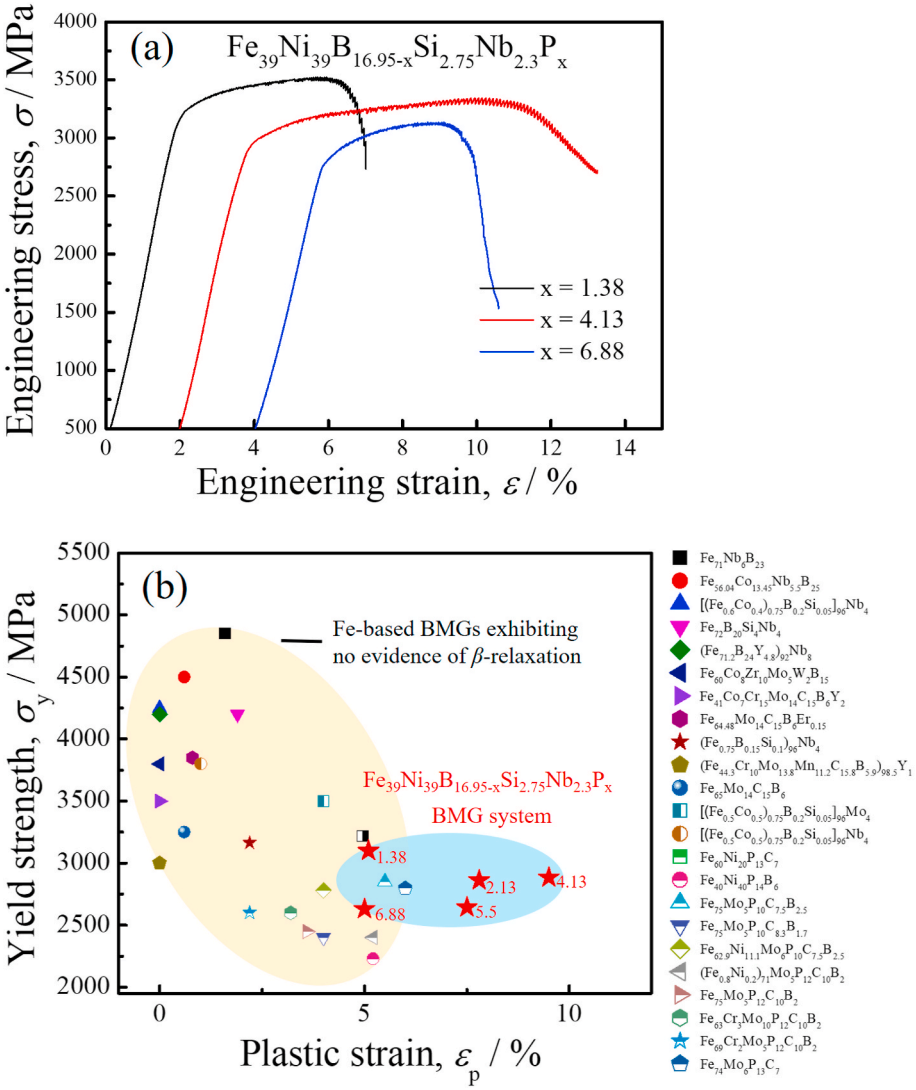

Fig. 9. (a) The engineering stress-strain curves of as-cast $Fe_{39}Ni_{39}B_{16.95-x}Si_{2.75}Nb_{2.3}P_x$ (x = 1.38, 4.13 and 6.88 at.%) BMGs at room temperature; (b) The compressive yield strength and the plastic strain of the representative Fe-based BMGs exhibiting no evidence of β-relaxation at room temperature. Data for a variety of different Fe-based BMGs are taken from Ref. [9]. For comparison, our new FeNi-based BMGs are included (labeled using red star).

a valley between the two highest fraction peaks in $Fe_{39}Ni_{39}B_{10.07}Si_{2.75}Nb_{2.3}P_{6.88}$ BMG, as shown in Fig. 6c. That means two separated areas may exist in this FeNi-based BMG, which is corresponding to the high ordered structure obtained from the synchrotron XRD results.

The contour maps in Fig. 7 show the spatial distribution of nanohardness values H of three FeNi-based BMGs over a 210 × 210 μm^2 square area. Here, we focus on the comparison of the spatial distribution between $Fe_{39}Ni_{39}B_{12.82}Si_{2.75}Nb_{2.3}P_{4.13}$ and $Fe_{39}Ni_{39}B_{10.07}Si_{2.75}Nb_{2.3}P_{6.88}$ BMGs, since $Fe_{39}Ni_{39}B_{15.57}Si_{2.75}Nb_{2.3}P_{1.38}$ BMG exhibits a lower degree of mechanical heterogeneity than them. As shown in Fig. 7b and c, it is interesting that the spatial distribution of $Fe_{39}Ni_{39}B_{12.82}Si_{2.75}Nb_{2.3}P_{4.13}$ and $Fe_{39}Ni_{39}B_{10.07}Si_{2.75}Nb_{2.3}P_{6.88}$ BMGs are obviously different, although they have the similar range of nanohardness values. For $Fe_{39}Ni_{39}B_{12.82}Si_{2.75}Nb_{2.3}P_{4.13}$ BMG, the valleys with low H values are surrounded by continuous zones with high H values, and uniformly spread throughout the areas. While for $Fe_{39}Ni_{39}B_{10.07}Si_{2.75}Nb_{2.3}P_{6.88}$ BMG, the nanohardness values are distributed by the agglomeration regions of low and high H values respectively, which are close together with each other.

Based on the analysis mentioned above, Fig. 8 shows the schematic diagram illustrating the atomic-scale structure of $Fe_{39}Ni_{39}B_{16.95-x}Si_{2.75}Nb_{2.3}P_x$ BMGs. As shown in the figure, when P content is 1.38 at. %, atoms are tightly stacked, and few loosely packed regions exists in this BMG. With the increase of P content, the internal arrangement of atoms become loose, leading to the enhancement of structural heterogeneity on the atomic scale. In addition, the spatial distribution of the loosely packed regions of $Fe_{39}Ni_{39}B_{12.82}Si_{2.75}Nb_{2.3}P_{4.13}$ BMG is uniform, while for the $Fe_{39}Ni_{39}B_{10.07}Si_{2.75}Nb_{2.3}P_{6.88}$ BMG, their distribution is relatively concentrated (indicated by black circle). This unique atomic-scale structure promotes multi-scale inhomogeneity at atomic to meso-scale in $Fe_{39}Ni_{39}B_{10.07}Si_{2.75}Nb_{2.3}P_{6.88}$ BMG.

In MGs, the loosely packed clusters are more likely to be activated than tightly packed ones. From above results, the $Fe_{39}Ni_{39}B_{10.07}Si_{2.75}Nb_{2.3}P_{6.88}$ BMG shows the highest structural heterogeneity from atomic to mesoscale, indicating the largest amount of loosely packed regions. Thus, the loosely packed regions in $Fe_{39}Ni_{39}B_{10.07}Si_{2.75}Nb_{2.3}P_{6.88}$ BMG are priority to cross an energy barrier and transfer to the supercooled liquid state due to the thermal fluctuations, leading to the increasing of loss modulus from the supercooled liquid, which presents as the pronounced β-relaxation [33,34]. In other words, the $Fe_{39}Ni_{39}B_{10.07}Si_{2.75}Nb_{2.3}P_{6.88}$ BMG exhibiting higher degree of heterogeneities displays a more pronounced β-relaxation behavior.

Recently, it has been confirmed that an inelastic distortion involving several atoms in MGs, which is regarded as the source of β-relaxation behavior, may also provides potential STZ sites [16]. Thereby, this $Fe_{39}Ni_{39}B_{16.95-x}Si_{2.75}Nb_{2.3}P_x$ BMGs are expect to have good plastic deformation ability. Fig. 9a shows the engineering stress-strain curves of as-cast $Fe_{39}Ni_{39}B_{16.95-x}Si_{2.75}Nb_{2.3}P_x$ BMGs tested under compression. All the samples exhibit high yield strength over 2600 MPa, whereas the plasticity increase from 5.1 to 9.8% with increasing P content, then decreases to 5% with further increase the P content to 6.88 at.%. In addition, Fig. 9b summarizes the yield strength versus plastic strain ranges for typical Fe-based BMGs with no evidence of β-relaxation, and $Fe_{39}Ni_{39}B_{16.95-x}Si_{2.75}Nb_{2.3}P_x$ BMGs developed in this work [9]. As shown in the figure, these $Fe_{39}Ni_{39}B_{16.95-x}Si_{2.75}Nb_{2.3}P_x$ BMGs shows excellent mechanical properties with plastic strain of 5.0–9.5% and yield strength of 2644–3217 MPa, which is an apparently breakthrough among Fe-based BMG family.

4. Conclusions

A plastic $Fe_{39}Ni_{39}B_{16.95-x}Si_{2.75}Nb_{2.3}P_x$ (x = 1.38, 2.75, 4.13, 5.5, 6.88 and 8.25 at.%) BMG system with plastic strains of 5.0–9.5% and yield strengthes of 2644–3217 MPa was successfully developed. It was found that the plasticity and the β-relaxation behaviors of the $Fe_{39}Ni_{39}B_{16.95-x}Si_{2.75}Nb_{2.3}P_x$ BMGs is correlated and are sensitive to the composition P content. Based on the analyses from the change in atomic-scale structure, the pronounced β-relaxation and plasticity of the BMGs is attributed to the structural heterogeneities, resulting in a large amount of loosely packed region. In addition, this structural heterogeneity also leads to the large plactic deformation ability of this Fe-based BMG system. The FeNi-based BMGs provide a model system for studying controversial issues such as the structural origin of the β-relaxation and the correlation between β-relaxation and properties in MGs.

CRediT authorship contribution statement

Jing Zhou: Data curation, Investigation, Writing – original draft, Roles/Writing - original draft. **Rui Zhao:** Investigation.

Declaration of competing interest

The authors declare that they have no known competing financial interests or personal relationships that could have appeared to influence the work reported in this paper.

Acknowledgment

This work was supported by the Guangdong Major Project of Basic and Applied Basic Research, China (Grant No. 2019B030302010), and the National Natural Science Foundation of China (Grant Nos. 51631003, 51871054 and U2032219). This research used the beamline 11-ID-C at APS, ANL, USA. APS is supported by the Department of Energy (DOE) Office of Science (DE-AC02-06CH11357).

References

[1] P. Duwez, S.C.H. Lin, Amorphous ferromagnetic phase in iron-carbon-phosphorus alloys, J. Appl. Phys. 38 (1967) 4096–4097.
[2] R. Hasegawa, Applications of amorphous magnetic alloys, Mater. Sci. Eng., A 375–377 (2004) 90–97.
[3] C. Suryanarayana, A. Inoue, Iron-based bulk metallic glasses, Int. Mater. Rev. 58 (2013) 131–166.
[4] A. Inoue, F.L. Kong, Y. Han, S.L. Zhu, A. Churyumov, E. Shalaan, F. Al-Marzouki, Development and application of Fe-based soft magnetic bulk metallic glassy inductors, J. Alloys Compd. 731 (2018) 1303–1309.
[5] K.P. Mizgalski, O.T. Inal, F.G. Yost, M. Karnowsky, Characterization of crystallization in Metglas 2826 MB alloy, J. Mater. Sci. 16 (1981) 3357–3364.
[6] A. Inoue, Y. Shinohara, J.S. Gook, Thermal and magnetic properties of bulk Fe-based, Mater. Trans., JIM 36 (1995) 1427–1433.
[7] C.T. Chang, B.L. Shen, A. Inoue, FeNi-based bulk glassy alloys with superhigh mechanical strength and excellent soft-magnetic properties, Appl. Phys. Lett. 89 (2006), 051912.
[8] A.D. Wang, M.X. Zhang, J.H. Zhang, H. Men, B.L. Shen, S.J. Pang, T. Zhang, FeNiPBNb bulk glassy alloys with good soft-magnetic properties, J. Alloys Compd. 536 (2012) S354–S358.
[9] J. Zhou, Q.Q. Wang, X.D. Hui, Q.S. Zeng, Y.W. Xiong, K.B. Yin, B.A. Sun, L.T. Sun, M. Stoica, W.H. Wang, B.L. Shen, A novel FeNi-based bulk metallic glass with high notch toughness over 70 MPa $m^{1/2}$ combined with excellent soft magnetic properties, Mater. Des. 191 (2020) 108597.
[10] J. Zhou, Q.Q. Wang, Q.S. Zeng, K.B. Yin, A.D. Wang, J.H. Luan, L.T. Sun, B.L. Shen, A plastic FeNi-based bulk metallic glass and its deformation behavior, J. Mater. Sci. Technol. 76 (2021) 20–32.
[11] F. Spaepen, A microscopic mechanism for steady state inhomogeneous flow in metallic glasses, Acta Metall. 25 (1977) 407–415.
[12] B.A. Sun, W.H. Wang, The fracture of bulk metallic glasses, Prog. Mater. Sci. 74 (2015) 211–307.
[13] B.A. Sun, L.P. Yu, G. Wang, X. Tong, C. Geng, J. Wang, J. Ren, W.H. Wang, Chaotic dynamics in shear-band-mediated plasticity in metallic glasses, Phys. Rev. B 101 (2020) 224111.
[14] H.B. Yu, W.H. Wang, K. Samwer, The β relaxation in metallic glasses: an overview, Mater. Today 16 (2013) 183–191.
[15] J.C. Qiao, J.M. Pelletier, Dynamic mechanical relaxation in bulk metallic glasses: a review, J. Mater. Sci. Technol. 30 (2014) 523–545.
[16] Z. Wang, B.A. Sun, H.Y. Bai, W.H. Wang, Evolution of hidden localized flow during glass-to-liquid transition in metallic glass, Nat. Commun. 5 (2014) 5823.
[17] H. Zhang, L. Zhu, S.S. Jiang, Y.G. Wang, F.G. Chen, Bending ductility of stress-relieved Fe-Zr-B metallic glasses with pronounced β-relaxation, J. Alloys Compd. 834 (2020) 155068.
[18] L.Z. Zhao, R.J. Xue, W.H. Wang, H.Y. Bai, The role of magnetic element Fe in pronounced slow β-relaxation in metallic glasses, Intemetallics 84 (2017) 148–152.

[19] J. Zhou, W.M. Yang, C.C. Yuan, B.A. Sun, B.L. Shen, Ductile FeNi-based bulk metallic glasses with high strength and excellent soft magnetic properties, J. Alloys Compd. 742 (2018) 318–324.
[20] A.P. Hammersley, S.O. Svensson, M. Hanflfland, A.N. Fitch, D. Hausermann, Two-dimensional detector software: from real detector to idealised image or two-theta scan, High Pres. Res. 14 (1996) 235–248.
[21] I.K. Jeong, J. Thompson, T. Proffen, A. Perez, S.J.L. Billinge, A program for obtaining the atomic pair distribution function from X-ray powder diffraction data, J. Appl. Crystallogr. 34 (2001) 536.
[22] W.C. Oliver, G.M. Pharr, An improved technique for determining hardness and elastic-modulus using load and displacement sensing indentation experiments, J. Mater. Res. 7 (1992) 1564–1583.
[23] W.L. Johnson, Bulk glass-forming metallic alloys: Science and technology, MRS Bull. 10 (1999) 42–56.
[24] A. Takeuchi, A. Inoue, Classification of bulk metallic glasses by atomic size difference, heat of mixing and period of constituent elements and its application to characterization of the main alloying element, Mater. Trans. 46 (2005) 2817–2829.
[25] S.J. Poon, G.J. Shiflet, F.Q. Guo, V. Ponnambalam, Glass formability of ferrous- and aluminum-based structural metallic alloys, J. Appl. Phys. 1–2 (2003) 1–9.
[26] J.C. Ye, J. Lu, C.T. Liu, Q. Wang, Y. Yang, Atomistic free-volume zones and inelastic deformation of metallic glasses, Nat. Mater. 9 (2010) 619–623.
[27] Z. Lu, W. Jiao, W.H. Wang, H.Y. Bai, Flow unit perspective on room temperature homogeneous plastic deformation in metallic glasses, Phys. Rev. Lett. 113 (2014), 045501.
[28] A.L. Greer, Y.H. Sun, Stored energy in metallic glasses due to strains within the elastic limit, Philos. Mag. A 96 (2016) 1643–1663.
[29] A.R. Yavari, A.L. Moulec, A. Inoue, N. Nishiyama, N. Lupu, E. Matsubara, W. J. Botta, G. Vaughan, M.D. Michiel, Å. Kvick, Excess free volume in metallic glasses measured by X-ray diffraction, Acta Mater. 53 (2004) 1611–1619.
[30] J.G. Wang, D.Q. Zhao, M.X. Pan, C.H. Shek, W.H. Wang, Mechanical heterogeneity and mechanism of plasticity in metallic glasses, Appl. Phys. Lett. 94 (2009) 31904.
[31] W.H. Wang, Correlation between relaxations and plastic deformation, and elastic model of flow in metallic glasses and glass-forming liquids, J. Appl. Phys. 110 (2011), 053521.
[32] W.H. Wang, Y. Yang, T.G. Nieh, C.T. Liu, On the source of plastic flow in metallic glasses: concepts and models, Intermetallics 67 (2015) 81–86.
[33] W.H. Wang, Dynamic relaxations and relaxation-property relationships in metallic glasses, Prog. Mater. Sci. 106 (2019) 100561.
[34] J.C. Qiao, Q. Wang, J.M. Pelletier, H. Kato, R. Caespo, E. Pineda, Y. Yao, Y. Yang, Structural heterogeneities and mechanical behavior of amorphous alloys, Prog. Mater. Sci. 104 (2019) 250–329.